Estimation of Forest Water Potential from Ground-Based L-band Radiometry

Jagdhuber, Thomas; Schmidt, Anne Sophie; Fluhrer, Anke; Chaparro, David; Jonard, François; Piles, Maria; Holtzman, Natan; Konings, Alexandra G.; Feldman, Andrew F.; Baur, Martin J.

DOI
10.1109/JSTARS.2025.3533567

Publication date
2025

Document Version
Final published version

Published in
IEEE Journal of Selected Topics in Applied Earth Observations and Remote Sensing

Estimation of Forest Water Potential from Ground-Based L-band Radiometry

Thomas Jagdhuber, *Senior Member, IEEE*, Anne-Sophie Schmidt, Anke Fluhrer, *Member, IEEE*, David Chaparro, *Member, IEEE*, François Jonard, *Senior Member, IEEE*, María Piles, *Senior Member, IEEE*, Natan Holtzman, Alexandra G. Konings, Andrew F. Feldman, Martin J. Baur, Susan Steele-Dunne, *Member, IEEE*, Konstantin Schellenberg, Harald Kunstmann

***Abstract*— Monitoring the water status of forests is paramount for assessing vegetation health, particularly in the context of increasing duration and intensity of droughts. In this study, a methodology was developed for estimating forest water potential at the canopy scale from ground-based L-band radiometry. The study uses radiometer data from a tower-based experiment of the SMAPVEX 19-21 campaign from April to October 2019 at Harvard Forest, MA, USA. The gravimetric and the relative water content of the forest stand was retrieved from radiometer-based vegetation optical depth. A model-based methodology was adapted and assessed to transform the relative water content estimates into values of forest water potential. A comparison and validation of the retrieved forest water potential was conducted with *in situ* measurements of leaf and xylem water potential to understand the limitations and potentials of the proposed approach for diurnal, weekly and monthly time scales. The radiometer-based water potential estimates of the forest stand were found to be consistent in time with $r_{Pearson}$ correlations up to 0.6 and similar in value, down to RMSE = 0.14 [MPa], compared to their *in situ* measurements from individual trees in the radiometer footprint, showing encouraging retrieval capabilities. However, a major challenge was the bias between the radiometer-based estimates and the *in situ* measurements over longer times (weeks & months). Here, an approach using either air temperature or soil moisture to update the minimum water potential of the forest stand (FWP_{min}) was developed to adjust the mismatch. These results showcase the potential of microwave radiometry for continuous monitoring of plant water status at different spatial and temporal scales, which has long been awaited by forest ecologists and tree physiologists.**

***Index Terms*— Soil plant atmosphere system, SPAC, vegetation water potential, vegetation, transmissivity, microwave radiometry, L-band, SMAP**

I. Introduction

In plants, water moves due to suction (and tension) created by a potential energy gradient from the soil into the atmosphere and by capillary action within plant vessels (Barceló-Coll et al., 1980; Cowan, 1965; Gardner, 1960 and 1965; Slayter and Taylor, 1960). Thus, water is driven by a pressure gradient which allows plants to take up water from the soils, transfer it through the xylem to the leaves, and finally release it into the atmosphere by transpiration through stomata.

Plant water potential is often described for individual plant components (e.g., leaf water potential) or referred to by the physical process to be analyzed, like matric and gravimetric water potential (Barceló-Coll et al., 1980). Since this study focuses on vegetation at the canopy scale, it will refer generically to forest water potential (FWP). The FWP depends on the soil water availability: a drier soil has a lower soil water potential, which can limit the plant water uptake and reduce the FWP (Van den Honert, 1948). Finally, at the leaf canopy-atmosphere interface, the dryness of the atmosphere (i.e., vapor pressure deficit) contributes to the pressure gradient in the plant. A drier atmosphere can induce higher transpiration and decreases the FWP which, in turn, may induce stomatal closure in order to reduce water losses at the cost of reducing plant carbon uptake (Jonard et al., 2011; Martínez-Vilalta & García-Forner, 2017). This way, FWP can control transpiration and photosynthesis rates (Venturas et al., 2017) by changing stomatal conductance. FWP is important for plant hydraulic behavior and is a key variable influencing the water, energy, and carbon cycles (Lambers et al., 2008; Martínez-Vilalta and Garcia-Forner, 2017). Including FWP information as a

Manuscript received: 16th of May 2024, reviewed: 30th of September 2024.

This work was supported with the MIT-Germany Seed Fund "Global Water Cycle and Environmental Monitoring using Active and Passive Satellite-based Microwave Instruments" and with the MIT-Belgium Seed Fund "Early Detection of Plant Water Stress Using Remote Sensing". D. Chaparro was supported by the Ramón Areces Foundation postdoctoral grant.

Thomas Jagdhuber, Anne-Sophie Schmidt, Anke Fluhrer, Konstantin Schellenberg and David Chaparro are with the Microwaves and Radar Institute, German Aerospace Center, 82234 Wessling, Germany (e-mails: {Thomas.Jagdhuber, Anne-Sophie.Schmidt, Anke.Fluhrer}@dlr.de).

T. Jagdhuber, H. Kunstmann and A. Fluhrer are also with the Institute of Geography, Augsburg University, 86159 Augsburg, Germany (email: harald.kunstmann@geo.uni-augsburg.de).

D. Chaparro is also with the Center for Ecological Research and Forestry Applications (CREAF), 08197 Cerdanyola del Vallès, Spain (e-mail: d.chaparro@creaf.uab.cat).

François Jonard, is with the Earth Observation and Ecosystem Modelling Laboratory, SPHERES Research Unit, Université de Liège (ULiege), 4000 Liège, Belgium (email: francois.jonard@uliege.be).

Natan Holtzman and Alexandra Konings are with Stanford University, School of Earth & Environmental Sciences, Stanford, CA 94305-2210, USA (emails: {nholtzma, konings}@stanford.edu).

Andrew Feldman is with the NASA Goddard Spaceflight Center, Biospheric Sciences Laboratory, Greenbelt, MD 20771, USA and the Earth System Science Interdisciplinary Center, University of Maryland, College Park, MD, USA. (e-mails: andrew.feldman@nasa.gov).

Martin J. Baur is with the University of Cambridge, Department of Geography, Cambridge, United Kingdom (email: mjb311@cam.ac.uk).

María Piles is with the Image Processing Lab, University of Valencia, 46980 Paterna, Spain (e-mail: maria.piles@uv.es).

Susan Steele-Dunne is with the Delft University of Technology, Department of Geoscience and Remote Sensing, Delft, The Netherlands (email: s.c.steele-dunne@tudelft.nl).

Konstantin Schellenberg is also with the Friedrich Schiller University Jena, Department for Earth Observation, Jena, Germany and with the Max Planck Institute for Biogeochemistry, Department Biogeochemical Processes, Jena, Germany (email: konstantin.schellenberg@uni-jena.de).

predictor can lead to improved estimates of stomatal conductance responses to drought (Anderegg et al., 2017; Bonan et al., 2014), enhance the capacity to understand transpiration responses to increased vapor pressure deficit under climate change (Liu et al., 2020), and allow enhanced land surface models by accounting for plant hydraulics (Christoffersen et al., 2016; Eller et al., 2020; Kennedy et al., 2019; Matheny et al., 2017). Detecting reductions in water potential is also essential to assess the risk of tree mortality (McDowell et al., 2008; Williams et al., 2013; Novick et al., 2016; Choat et al., 2018) and of fire (Nolan et al., 2020), as well as to explain variations in tree growth and in forest phenology (Xu et al., 2016).

FWP monitoring helps to predict an ecosystems' response to actual and future climate extremes. However, current FWP measurements are mainly limited to *in situ* efforts, meaning FWP is sparsely measured in space and time, given destructive and expensive techniques (Novick et al., 2022). Specifically, manual plant water potential observations are mostly taken with pressure chambers (Scholander et al., 1965; Rodríguez-Domínguez et al., 2022) and psychrometers (Edwards and Dixon, 1995), among other techniques (Dixon and Tyree, 1984; Balling and Zimmerman, 1990; Melcher et al., 1998).

Due to these limitations, only a few a databases of plant water potential measurements exist (e.g., Choat et al., 2012). Still, they are site-specific and are not continuously sampled in time. Data on plant water potential are rarely collected (PsiNet) and not standardized in databases and networks. Moreover, scaling water potential measurements from the individual plant to entire forests or ecosystems remains a challenge (Konings et al., 2021; Novick et al., 2021). Satellite sensors have the potential to measure vegetation conditions and fulfill the scientific need for global water potential estimates with a high temporal resolution (e.g., less than a week). So far, optical vegetation indices (VIs) from satellite and airborne platforms have shown promising results even with commercial applicability in croplands (Helman et al., 2018; Zarco-Tejada et al., 2013; Lin et al., 2020) and in some natural landscapes (Palmer et al., 2008 and 2010; Hwang et al., 2017), at local scales. To the authors' knowledge, however, regional-scale or larger-scale studies are lacking so far. In addition, optical VIs are limited by clouds and sun-glint effects and, importantly, are only sensitive to the vegetation properties at the top of the canopy leaves (Konings et al., 2019; Zarco-Tejada et al., 2003). Moreover, VIs that measure pigment (chlorophyll) variations and therefore photosynthetic activity are even less sensitive to vegetation water content dynamics directly.

To overcome these issues, the global ecological remote sensing community has recently explored the capacity of passive microwave measurements to sense the water potential of vegetation. Such measurements have the advantage of being sensitive to plants' water content, structure, and biomass. In passive microwave radiometry, this information is integrated in a parameter named vegetation optical depth (VOD). VOD refers to the attenuation that the vegetation canopy exerts over the land emissions in the microwave range of the electromagnetic spectrum (Ulaby & Long, 2014; Meyer et al., 2018). At higher microwave frequencies (i.e., X-band, ~10 GHz, and Ku-band, ~15 GHz), the VOD is sensitive to the water content in the upper canopy (due to lack of canopy sensing depth at these frequencies). It has been related to the live fuel moisture content ($LFMC$; Forkel et al., 2022; Chaparro et al., 2024) or to the isohydricity behavior of vegetation (Konings and Gentine, 2017) at global scale. At lower frequencies (i.e., L-band, ~1 GHz, which senses nearly all the canopy layers given its longer wavelength), a recent forest study has revealed that VOD is correlated with the xylem water potential, and that it shows a similar diurnal cycle to *in situ* xylem and leaf water potential (Holtzman et al., 2021).

Ideally, the water component of VOD could be disentangled from the components of biomass and structure to evaluate the water status of plants more precisely. To achieve this goal, a common strategy is to derive the relative water content (RWC) by normalizing VOD in time, and assuming the biomass is constant at yearly time scales (Rao et al., 2019; Martínez-Vilalta et al.; 2019).

Another strategy consists of estimating vegetation moisture mg (in [kg/kg]) from VOD using information from additional sensors and deriving RWC from minimum and maximum values of mg. This approach has been applied at local (Meyer et al., 2019) and continental scales (Fink et al, 2018, Chaparro et al., 2024) using active microwaves and lidar to account for the biomass and vegetation structure imprint on VOD. From each of the approaches, the obtained RWC can be used to estimate FWP by applying pressure-volume curves (Konings et al., 2019; Konings et al., 2021; Jagdhuber et al., 2022).

The goal of this study is therefore to derive FWP dynamics using tower-based, local-scale L-band VOD measurements coupled to pressure-volume curves. These time series of FWP are compared with *in situ* xylem and leaf water potential measurements. Thus, it is hypothesized that the proposed approach leads to a first ground-based FWP retrieval from VOD. Moreover, the diurnal, weekly and up to monthly dynamics have been assessed to understand the ability to estimate water potential on different time scales. The study sets the path for enabling future retrievals that could be based on passive microwave sensors currently in orbit, like the Advanced Microwave Scanning Radiometer 2 (AMSR-2), and the L-band radiometers on the Soil Moisture and Ocean Salinity (SMOS) and the Soil Moisture Active-Passive (SMAP) missions. Such FWP retrievals, if provided at larger spatial scales (e.g., regional), would allow to study forest water relations at a scale that was not possible before, and would ease finding forest drought-induced mortality thresholds in space and time to know when and where forests are at risk of die back.

II. Test Site and Experimental Data

Previous to the study, a ground-based acquisition setup was designed to estimate *FWP* and established within the research site of Harvard University (Holtzman et al., 2021). The forest test site is located on Prospect Hill within Harvard Forest (42.535° N, 72.174° W), MA, USA. It is a temperate deciduous forest dominated by red Oak (*Quercus rubra*) in a humid continental climate (Holtzman et al., 2021). An overview of the measurement setup is shown in Fig. 1.

As part of the SMAP Validation Experiment 2019-2021 (SMAPVEX 19 -21), *in situ* measurements for soil, plants and atmosphere were carried out between 28th of April and 17th of October 2019 (Colliander et al, 2020). These measurements

include soil moisture and soil temperature at 5 cm and 10 cm depth, tree xylem permittivity and xylem water potential (XWP), leaf wetness and leaf water potential (LWP), and air temperature. Not all *in situ* measurements could be conducted continuously along the campaign period. Three intensive measurement periods took place between 9th – 18th of July, 5th – 13th of August and 7th – 26th of September, 2019 with almost all sensors in operation.

An L-band (1.4 GHz) radiometer (Potter Horn, PR-1475, Radiometrics Inc.) was mounted at 28 m height on a tower pointing with an incidence angle of 40° into the forest canopy with about 21 m to 23 m height (cf. Fig. 1). This incidence angle is consistent with the current spaceborne SMAP radiometer. The ground footprint dimensions are 25 m by 20 m, defined by the half power beam width (-3 dB) of the antenna at 30° opening angle (Holtzman et al., 2020). The instrument conducted hourly measurements of dual-polarimetric, i.e. horizontally (H) and vertically (V) polarized brightness temperatures with an accuracy of 2 K (Rowlandson et al., 2018). Only V-polarized measurements were used in this study, as H-polarized data showed unexplained fluctuations, as stated previously in Holtzman et al. (2021). Further details on radiometer operation and *in situ* measurements are provided in Holtzman et al. (2021) and Roy et al. (2020).

The VOD-estimates, also included in Holtzman et al. (2020), were calculated using a single channel V-polarized (SCA-V) retrieval algorithm based on a zeroth order radiative transfer model (Mo et al., 1982; Entekhabi et al., 2014). In contrast to the classical SCA-V retrieval approach in the SMAP baseline algorithm (Entekhabi et al., 2014), *in situ*-based soil moisture was here input to the algorithm, and the radiative transfer equation solved for VOD, like in Baur et al. (2019). Radiometer measurements were made at times lacking thermal equilibrium between the soil and vegetation (such as appropriately assumed at 6 am for the SMAP baseline algorithm (Entekhabi et al., 2014)). Therefore, the soil and canopy temperatures were taken from the *in situ* measurements of Holtzman et al. (2020).
For canopy temperature, the air temperature at one-meter height within the forest stand was used, because direct canopy measurements were not available. This temperature substitution was investigated by Holtzman et al. (2021) and was shown to be sufficient. For parameterization of soil roughness and scattering albedo, the standard values of Holtzman et al. (2021), deduced from the SMAP soil moisture product for temperate broadleaf forests, were taken (soil roughness: $h = 0.16$, scattering albedo: $\omega = 0.05$).

Figure 2 presents the VOD time series from 10th (noon) to 18th (11 pm) of July, 2019 during the first intensive measuring period together with *in situ* data of the XWP [MPa], measured for one tree in the stand. The VOD time series in Fig. 2 shows a diurnal dynamic of temperature (driven by the solar cycle, cf. Fig. 3 top) similar to the XWP dynamics in most days (with few exceptions, e.g. July 17th). An overall decreasing trend was observed similar to the hydro-dynamics of the in situ soil moisture (cf. Fig. 3 bottom) along multiple days up to one week. Figure 3 provides an *in situ*-based overview on the water and energy status and dynamics for the intensive measurement campaign in July 2019 (August & September campaigns in the Supplement). It reveals how the light and water conditions influenced the *in situ* XWP measurements and remote sensing (VOD) plant water dynamics during the intensive campaign period. Diurnal soil and air temperature minima and maxima are opposite to that of the xylem water potential confirming the interplay between light and water.

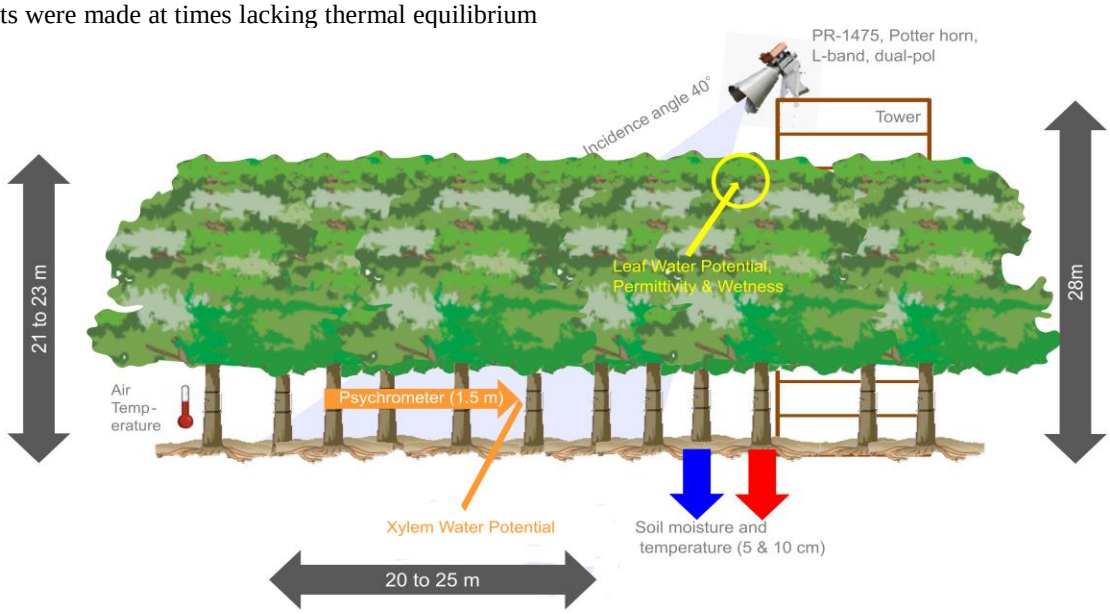

Fig. 1. Overview of the measurement setup at the Harvard Forest, MA test site during the SMAPVEX 19-21 campaign: The tower-based radiometer with its slanted observation geometry sensing into the forest complemented by *in situ* measurements on air and soil temperature, soil moisture, xylem and leaf water potential, leaf permittivity and leaf wetness (Holtzman et al., 2021; Clark et al., 2018).

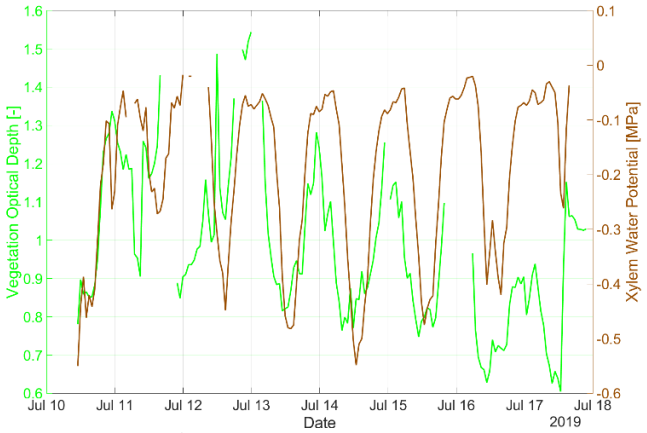

Fig. 2. Time series of L-band radiometer-retrieved vegetation optical depth (VOD) [-] and *in situ*-measured xylem water potential (XWP) [MPa] in the temperate forest stand during the intensive measurement campaign in July 2019 at Prospect Hill (Harvard Forest).

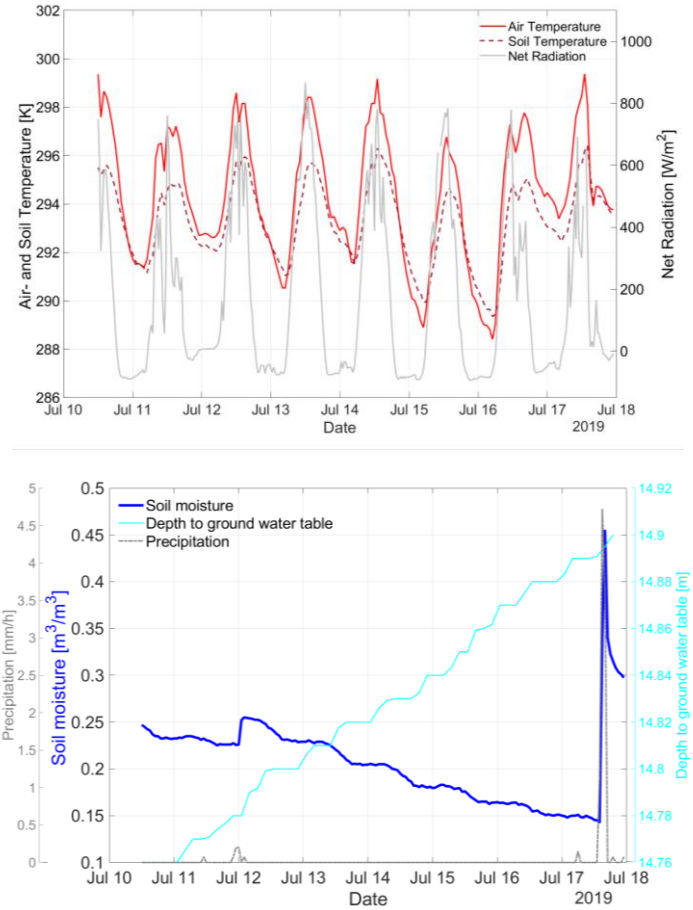

Fig. 3. Time series of *in situ*-measured soil and air temperature [K] and net radiation [W/m²] (top) as well as surface soil moisture [m³/m³], precipitation [mm/h] and depth to ground water table [m] (bottom) in the temperate forest stand during the intensive measurement campaign in July 2019 at Prospect Hill (Harvard Forest).

III. Methodology of Retrieving Forest Water Potential from Vegetation Optical Depth

Since VOD represents the attenuation of the L-band electromagnetic waves by the forest canopy, it is not only sensitive to the water component of the canopy, but also to its biomass and structure characteristics. Here, a simple, physics-based and analytically solvable model of VOD from Jackson and Schmugge (1991) is used to disentangle the water component from the radiometer-based VOD.

A. *From VOD to gravimetric water content of vegetation m_g*

VOD is linked to the gravimetric water content of vegetation m_g, in kilogram of water per kilogram of wet biomass [kg/kg]. The m_g can be extracted by the comparison of forward modelled VOD with data-retrieved VOD as initially applied in Meyer et al. (2019) and further refined in Chaparro et al. (2024). The VOD model in (1) – (3) needs information on the vegetation height h_{veg} [m], the vegetation volume fraction δ_i [m³/m³] (volume of plant material per volume of air as seen by microwave sensors), the main plant structure (here: random orientation of plant components), the shape of the major plant component (here: spheroids) and the wavelength of the observing system [m] (here: L-band, λ = 0.21 [m]) as input variables (Chaparro et al., 2024; Meyer et al., 2019; Jackson and Schmugge, 1991; Schmugge and Jackson, 1992; Ulaby and El-Reyes, 1987):

$$VOD = 4 \cdot \pi \cdot \frac{h_{veg}}{\lambda} \cdot Im\left[\sqrt{\epsilon_{can}}\right], \quad (1)$$

ϵ_{can} is the dielectric constant of the canopy:

$$\epsilon_{can} = \epsilon_h + \delta_i \frac{(\epsilon_i - \epsilon_h)(\epsilon^* + \epsilon_i)}{3(\epsilon_i + \epsilon^*)}, \quad (2)$$

where ϵ_h [-] and ϵ_i [-] are the permittivity of the host medium and the inclusions, respectively. The host medium is assumed to be air ($\epsilon_h = 1$). In addition, it is assumed that $\epsilon^* = \epsilon_h$, as δ_i is expected to be small ($\delta_i \ll 1$) (Ulaby and El-Reyes, 1987). Equation (2) is derived from Ulaby and Long (2014) assuming that the spheroids accounting for the plant material structure are randomly oriented needles, in agreement with Meyer et al. (2019) and Chaparro et al. (2021).

The permittivity of the plant material can be linked to m_g by the Debye-Cole dual dispersion dielectric mixing model (Ulaby and El-Reyes, 1987):

$$\epsilon_i = \epsilon_{fw} v_{fw} + \epsilon_{bw} v_{bw} + \epsilon_r, \quad (3)$$

where ϵ_{fw} and ϵ_{bw} are the permittivity of free water and bound water within the plants, respectively. The terms v_{fw}, v_{bw} and ϵ_r are the volume fractions of free and bound water as well as the residual permittivity component. The latter three parameters are a function of m_g, the salinity and the temperature of the plant material (cf. Ulaby & El-Reyes, 1987 for details). The salinity and the temperature are fixed to 10 [‰] and 22 [°C], as done in previous studies (Ulaby and El-Reyes, 1987; Chaparro et al., 2024). Details of this dielectric mixing model are described in Ulaby and El-Reyes (1987). The m_g-value minimizing the difference between the modelled VOD in (1) – (3) and the radiometer-derived VOD is chosen as the result.

B. *From gravimetric water content of vegetation m_g to relative water content RWC*

Next, m_g is converted into the relative water content (RWC) using dry moisture-minimum ($m_{g_{min}}$) and full turgor moisture-maximum ($m_{g_{max}}$) references (Smart and Bingham, 1974):

$$RWC_{mg} = \frac{m_g - m_{g_{min}}}{m_{g_{max}} - m_{g_{min}}} \cdot 100\ [\%]. \quad (4)$$

The definition of the extremes (min, max) sets the boundaries of the relative water dynamic and therefore the extent of the dynamic when moving to a relative metric. The time period for finding the extreme values may reach from diurnal (24h) up to seasonal (e.g., summer, winter) or even up to multi-annual scale, but will be set to diurnal ranges for the following analyses. Moreover, VOD can be directly used to calculate RWC in case of stable biomass and canopy structure conditions along the observation period (Rao et al., 2019):

$$RWC_{VOD} = \frac{VOD - VOD_{min}}{VOD_{max} - VOD_{min}} \cdot 100\ [\%]. \quad (5)$$

RWC_{VOD} will serve as a benchmark to RWC_{mg} and as a relative indicator of biomass/structure-bias between (4) and (5).

C. *From relative water content RWC to forest water potential FWP*

RWC is then converted into forest water potential (FWP) by the sigmoidal function of Zweifel et al. (2001):

$$FWP_{mg} = \frac{FWP_{min}}{e^{\frac{-k_1 + RWC}{k_2}} + 1}\ [\text{MPa}], \quad (6)$$

where FWP_{min} is the minimum forest water potential of the RWC-FWP relationship. Parameters k_1 [-] and k_2 [-] are empirical (site- and plant-specific) representing the inflection point and the rate of change between RWC and FWP. These parameters depend on hydraulic components of the vegetation and local climate within the stand.

The advantage of this functional form compared to alternative ones (e.g., Mirfenderesgi et al. (2016)) is its easy to adapt and parsimonious character (k_1, k_2, FWP_{min}), to enable water potential estimation. Figure 4 illustrates the adaptivity of this relationship for a slow (k_1=55, k_2=10), an intermediate (k_1=68, k_2=7.5), and a rapid (k_1=81, k_2=5) rate of RWC-to-FWP change, starting from an FWP_{min} of -2.5 [MPa].

In this work, the three parameters (k_1, k_2, FWP_{min}) were optimized jointly using the on-site XWP (psychrometer) measurements of the first intensive observation period in July 2019. The optimization results in k_1 and k_2 of 25 and 31, respectively. Both were fixed throughout the analyses of the remaining time series. This was supported by a sensitivity analysis (not shown) indicating that the most sensitive parameter in the RWC-FWP relationship is FWP_{min} compared to k_1 and k_2. FWP_{min} was first set to the minimum of XWP of the first diurnal cycle and then updated dynamically through time.

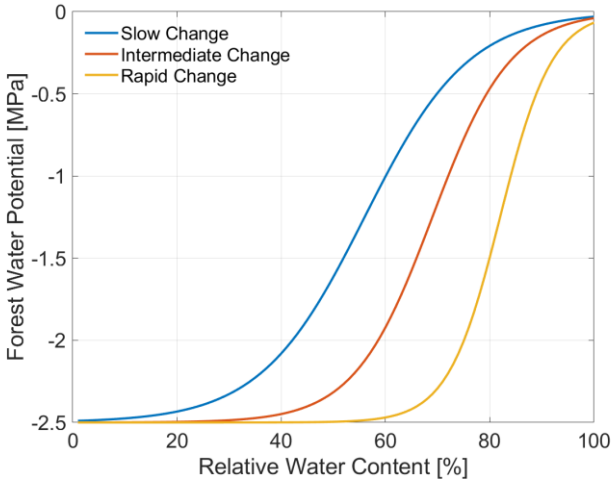

Fig. 4. Conceptual view on the RWC-FWP relationship for forest under slow, intermediate and rapid change rate, adapted from Zweifel et al. (2001); calculated with (6) using FWP_{min}= 2.5 [MPa], $k1_{slow}$= 55 & $k2_{slow}$= 10, $k1_{intermediate}$= 68 & $k2_{intermediate}$= 7.5, $k1_{rapid}$= 81 & $k2_{rapid}$= 5.

D. *Dynamization of FWP by updating FWP_{min}*

The dynamic update of FWP_{min} was based on two commonly available and continuously recorded *in situ* measurements: surface soil moisture θ_s [m³/m³] and air temperature T [K] at 1 [m] height, as they are key factors in constraining plant water uptake and plant water loss, respectively. In more general terms, these dynamic updates of FWP with soil moisture as well as with air temperature enable the extrapolation of the FWP estimation to longer periods, in terms of weeks and months towards seasons.

For FWP_{min}-update, θ_s and T were tested individually to understand the benefit of a mass-related variable (θ_s) and an energy-related variable (T). In this study, this FWP_{min}-update was developed by adapting the numerator of (6). Equations (7) and (8) define the proposed FWP_{min}-updated equations.

The soil moisture-based FWP_{min}-update is expressed by:

$$FWP = \frac{FWP_{min} + |FWP_{min}| * \frac{\partial \theta_s}{\partial t}}{e^{\frac{-k1 + RWC}{k2}} + 1}\ [\text{MPa}], \quad (7)$$

where $\frac{\partial \theta_s}{\partial t}$ represents the rate of change in soil moisture, $\partial \theta_s$, along time interval, ∂t, that is multiplied with the increment of $|FWP_{min}|$ from the previous time step. Soil moisture-based FWP_{min}-update is done in steps of five hours using the preceding five-hour time period for calculus. Shortly after a significant rain pulse, $\frac{\partial \theta_s}{\partial t}$ can grow as large as 0.5 $[\frac{m^3}{m^3}/h]$ or higher. In these exceptional cases of 50% increase within the preceding time interval, a data-calibrated cap factor of 0.7 was used for the respective rate of change to control updates of FWP_{min} and prevent overshooting.

Corresponding to (7), (6) can be also adapted for an air temperature-based FWP_{min}-update:

$$FWP = \frac{FWP_{min} + |FWP_{min}| * (-\frac{\partial T}{\partial t} * k_3)}{e^{\frac{-k1 + RWC}{k2}} + 1}\ [\text{MPa}], \quad (8)$$

including the inverse rate of change $-\frac{\partial T}{\partial t}$ in air temperature, ∂T, along time interval, ∂t, (since air temperature and water potential are negatively correlated), and a factor k_3 [-] to normalize for the distinctively different value ranges between XWP and T:

$$k_3 = \frac{XWP_{max} - XWP_{min}}{T_{max} - T_{min}}. \quad (9)$$

The $-\frac{\partial T}{\partial t} * k_3$-term in (8) was multiplied with the last increment of $|FWP_{min}|$ to update FWP_{min}. The air temperature-based FWP_{min}-update was conducted in 24h-intervals (from one daily mean value to the next). Daily updates were used instead of sub-daily ones to decouple FWP_{min}-dynamics from the diurnal solar cycle. In some cases, strong alterations in water potential can happen during the day. Then, the short-term change in water potential is so strong that the transient and mild changes in daily air temperature update would not cover it. At these points in time (hereafter named breakpoints), the temperature-based FWP_{min} was re-calibrated with the minimum of XWP *in situ* measurements at the day of the breakpoint.

IV. Results and Assessment of Forest Water Potential Estimation

In the following, FWP-estimates are shown for the intensive measurement periods in July, August and September 2019. First, the different intermediate variables along the retrieval process are presented (cf. Section III). Since all variables were retrieved from tower-based L-band microwave radiometry observing an entire forest canopy (vertical extent), they can only be considered as effective canopy-scale variables compared to their location-based *in situ* counterparts given their spatial scale mismatch (Konings et al, 2021).

A. m_g retrieval results

The retrieval of m_g is shown in Fig. 5 for the intensive measurement period in July 2019. It includes an average stand height of 21 m (top of canopy) provided by airborne Lidar scanning (Sullivan et al., 2017). Since δ is generally not known for an L-band tower-based radiometer and optics-based laser scanning does not inform about δ seen by microwaves, a range of naturally occurring volume fractions covering the full physical range of δ from 0.001 to 0.9 was tested representing the vegetation structure and dry biomass influence on VOD.
In Fig. 5, the mean of m_g for the range of δ is located around 0.1, whereas the extremes of δ led to m_g-values from 0.03 to 0.6. The higher δ is, the more the temporal dynamics of m_g deviate from VOD. Thus, for high vegetation volume fractions m_g- and VOD-dynamics differed significantly. This led to almost no dynamics in m_g for maximum δ, because vegetation structure and dry biomass dominated VOD (dashed red curve in Fig. 5). In contrast, at minimum δ, VOD dynamics are predominantly caused by water content variations leading to strong dynamics in m_g (solid red curve in Fig. 5). Also, higher values of δ led to lower values of m_g, while lower values of δ increase the estimated vegetation moisture. Importantly, choosing the minimum δ (i.e., δ = 0.001) was appropriate because it led to $m_g$values between 0.3 and 0.6 [kg/kg].

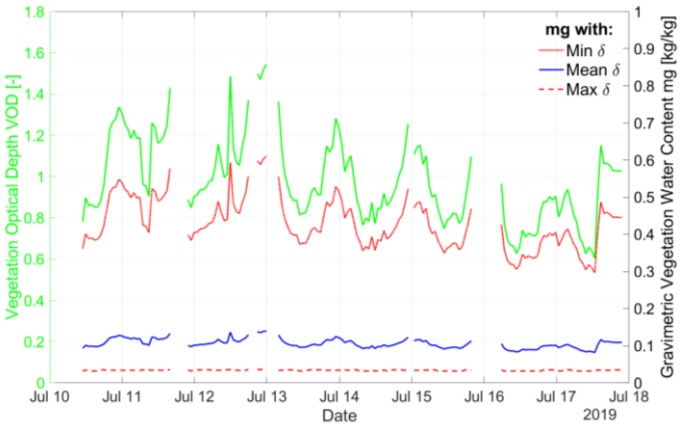

Fig. 5. Time series of m_g-estimates (blue and red colors) compared to their retrieval input parameter, vegetation optical depth (green color). Variation between the blue and red curves is due to the assumed vegetation volume fraction δ [-]: min=0.001 (red solid), max=0.9 (red dashed) and mean (blue) are calculated from minimum to maximum values.

This is in range with the average vegetation moisture conditions according to *in situ* data from oak species both at global scale (Yebra et al., 2019; n = 11118; mean m_g= 0.49 [kg/kg]; std. m_g= 0.07 [kg/kg]) and, in specific regions such as the (drier) French Mediterranean area (Duché et al., 1996; n = 2007; mean m_g= 0.44 [kg/kg]; std. m_g= 0.03 [kg/kg]). In addition, choosing such low values for microwave observations agrees with literature (Choudhury and Pampaloni, 1995; Schmugge and Jackson, 1992; Ulaby et al., 1983; Wigneron et al., 1993).

B. RWC retrieval results

Since δ is arduous to assess with experimental measurements at canopy scales and not known, neither generally nor for this study, RWC was calculated in two ways: first as RWC-m_g according to (4), second as RWC-VOD substituting m_g with VOD as shown in (5). Moreover, the minimum and maximum of the respective time series of the daily (24h) extreme values is used in (4).

Using VOD instead of m_g in (4) had negligible effects when daily minimum and maximum values were considered (not shown). It is understood that VOD seems to be an equivalent predictor compared to m_g for plant water content for shorter studies (less than one month) (Holtzman et al., 2021). This might be the case since dry biomass and vegetation structure (detectible at L-band) varied relatively little at Prospect Hill (Harvard Forest) during the intensive measurement weeks in July, August and September, respectively.

C. FWP retrieval results

In the final processing step, an effective (as seen by an L-band radiometer system), canopy-scale FWP is calculated from the retrieved RWC-estimates using the individual RWC-FWP relationships presented in equations (6) to (9). In Fig. 6, the

FWP-estimates based on RWC from m_g are compared with *in situ* measurements of XWP (brown curve) and LWP (blue dots). The temporal (daily) dynamics of the three potentials (FWP, XWP, LWP) show a promising concurrency in time, but a mismatch in absolute values (daily range of potentials). FWP-m_g was calculated in Fig. 6 with (6) assuming a time static FWP_{min} along the week in July. This resulted in a constant lower boundary of FWP, which never reached values below -0.4 [MPa]. This FWP estimation method is called "static FWP_{min}" retrieval hereafter. In this static approximation, the constant FWP_{min} was set to -2.5 [MPa]. This value was obtained from the models of Zweifel et al. (2001), which are based on spruce (*Picea abies*). In the case of oak (*Quercus rubra*), the value chosen is also realistic for a healthy forest. This species has been found to start stomatal closure at LWP = -1.85 [MPa] (Abrams et al., 1990), and change the xylem morphology due to progressive collapse at LWP between -2 [MPa] and -3 [MPa] (Zhang et al., 2016). Risk of cavitation for this species has been found at XWP = -3.10 [MPa] (Maherali et al., 2006) and, for oaks in general, it occurs at XWP = -4 [MPa] (median value from 14 species in supplement data of Choat et al., 2012).

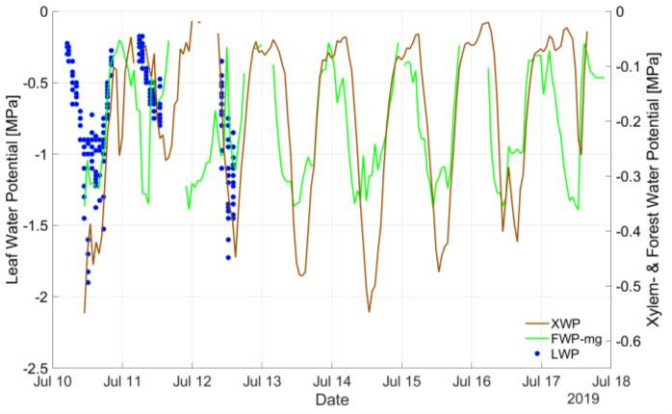

Fig. 6. Comparison of *in situ* measurements (xylem water potential: brown curve; leaf water potential: blue dots) and radiometer-based estimates (green curve) of FWP, assuming a static FWP_{min}.

For dynamization along time, FWP_{min} is updated continuously over time according to (7) – (9) to serve as a dynamic variable in (6). A time-dynamic FWP_{min} was essential to guarantee the flexibility of FWP in terms of absolute values and different tension levels. RWC as input variable in (6) is a relative measure and only FWP_{min} sets the lowest value in the FWP-range transforming into an absolute measure.

The update can be organized by incorporating available auxiliary data that is recorded independently and is easily available from contemporary *in situ* monitoring, like soil moisture (mass-based update) as in (7) or air temperature (energy-based update) as in (8) – (9).

The analysis of weekly FWP dynamics is shown in Fig. 7. It presents the retrieved FWP using either the static FWP_{min} (green curve), or the time-variable FWP_{min}, either updated by soil moisture (light green curve) or air temperature (dark green curve) *in situ* measurements.

In the July period, the soil moisture adaption led to an increasing daily dynamic of FWP especially around 16th to 18th of July that was not captured by XWP (brown curve). The air temperature adaption led to a similar dynamic of FWP in July, and stayed close to the static FWP dynamics. In contrast, the August period revealed that the temperature adapted FWP was able to trace partially (-1.6 to -0.2 [MPa]) the large dynamic range of the XWP (-1.9 to -0.2 MPa) in the beginning of the week (5th to 7th of August).

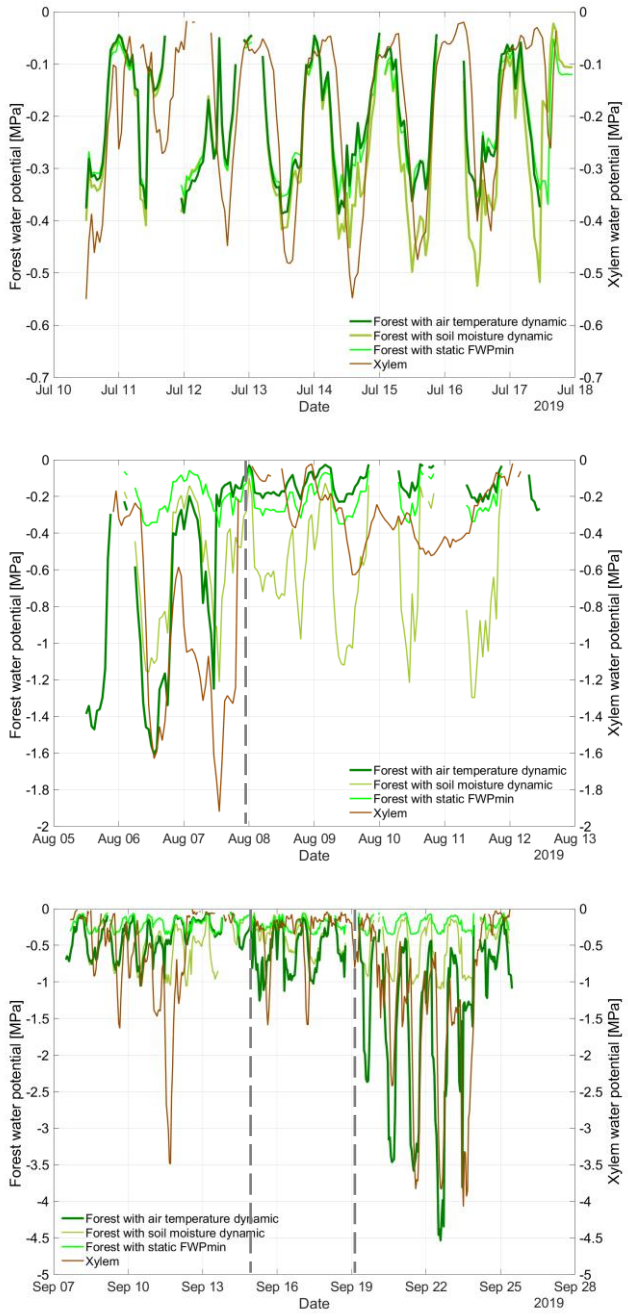

Fig. 7. Comparison of water potentials for the different intensive measuring periods in 2019 (Top: July, Middle: August, Bottom: September): Estimated from remote sensing (FWP in green for static (bright color) and dynamic FWP_{min} (middle and dark color))), measured *in situ* water potential XWP (from xylem; in brown); gray dashed bars indicate the break points (cf. Section III).

There is a distinct precipitation phase (> 5 [mm]) in the afternoon of the 7th (see Fig. S1 in the Supplement) leading to a soil moisture level close to 40 [vol.%] around midnight. After this period (8th to 12th of August) XWP stayed close to saturation (-0.61 [MPa] to zero [MPa]). Qualitatively, this was detected by both, the static and the temperature-based, FWP approaches.

The soil moisture-adapted FWP showed larger variation compared to XWP along these days. Additionally, daily variations of soil moisture-adapted FWP increased towards 13th of August due to constantly decreasing soil moisture down to values close to 20 [vol.%] (see Fig. S1 in the Supplement).
In contrast, the static FWP stayed between -0.4 [MPa] and zero [MPa], which is expected, since FWP_{min} is a constant calibrated once from *in situ* XWP on 10th of July. The same is true for the period in September and clearly indicates the importance of a time dynamic FWP_{min} to meet the changing hydrological conditions along the week and throughout the year.

In the September period (Fig. 7 bottom), the daily minima of XWP showed the lowest values (down to -4.5 [MPa]) of all intensive measurement periods. Here, two rain events occurred on 15th and 23rd of September (cf. Fig. S1) leading to reduced (less negative) water potentials afterwards. In addition, air temperature rose significantly from 19th to 23rd of September, depicted in Fig. S1. The temperature adapted FWP also demonstrates the capability to reach down to the lowest (most negative) water potentials in that week and indicates the strength of the break point mechanism for the temperature-based update (cf. Section III). However, this is not the case for the soil moisture adapted FWP which stayed between -1.0 and zero [MPa] and followed the hydro-dynamics guided by the two rain events during the intensive period.

D. Evaluation of the FWP retrievals

For the intensive measurement period in July, results based on the static FWP_{min} show FWP-values ranging between zero and -0.4 [MPa], like the dynamic range of *in situ* XWP (zero to -0.5 [MPa]) and shorter in dynamic range than *in situ* LWP (zero to -2 [MPa]). This suggests that FWP derived at L-band is sensitive to deeper canopy layers (trunk and branches) as well as to leaves (see subsection IV.E for detailed analysis), which was expected due to the larger sensing depth at this wavelength and agrees with literature (Konings and Gentine, 2017; Li et al., 2021; Schmidt et al., 2023). The dynamic range captured by the FWP-estimates, as well as that of the *in situ* data, show that the oak stand is generally not affected by hydric stress during July 2019, since there is no gradual decrease in the pre-dawn water potential towards higher moisture deficits (more negative FWP -values). The results demonstrate, however, a constant minimum value of FWP = -0.4 [MPa], which means that the static method is not able to capture dynamics at the lower edge of the *in situ* XWP time-series due to the FWP_{min}-fixation over time (see FWP-curve in Figs. 6 & 7).

It is confirmed here that FWP_{min} needed to be updated for each individual time increment to enable the estimation of realistic FWP-values. We further validate the proposed two guiding variables (soil moisture & air temperature) for this estimation. The dynamic FWP_{min} values were also within the expected range (between -0.5 [MPa] and -6 [MPa]). For the lower limit case, note that the resulting FWP did not reach this minimum of -6 [MPa], which can only be found in some oak species (Choat et al., 2012).

At hourly to weekly timescales (cf. Fig. 7 and Tab. I), results revealed a moderate capacity to track XWP variability using the air temperature dynamic approach ($0.48 < r < 0.60$), outperforming the capacity of the static and soil moisture approaches ($0.13 < r < 0.51$). Importantly, the temperature-driven approach for FWP was able to capture sudden and large declines (down to -4 [MPa]) of the *in situ* XWP (September 20th - 24th, Fig. 7) due to its break point mechanism (cf. Section III). This suggests that at coarser scales the proposed approach could help to capture cavitation-prone hydraulic conditions in forests.

TAB. I: SPEARMAN AND PEARSON CORRELATION COEFFICIENTS AND ROOT MEAN SQUARE ERROR (RMSE) FOR COMPARISON OF FWP AND XWP TIME SERIES ALONG THE THREE INTENSIVE PERIODS (JULY, AUGUST, SEPTEMBER) IN 2019.

Retrieval Method	Intensive measuring period	Rank Correlation (Spearman)	Linear Correlation (Pearson)	RMSE [MPa]
Static FWP_{min}	July	0.39	0.49	0.14
	August	0.08	0.13	0.61
	September	0.08	0.26	1.09
Soil moisture based FWP_{min}	July	0.43	0.51	0.15
	August	0.12	0.14	0.56
	September	0.23	0.48	0.90
Air temp-erature based FWP_{min}	July	0.38	0.48	0.14
	August	0.46	0.59	0.48
	September	0.42	0.60	0.83
VOD (no FWP retrieval)	July	0.30	0.32	-
	August	0.54	0.65	-
	September	0.62	0.69	-

E. Diurnal dynamics of FWP

After investigating the weekly dynamics in Fig. 7, the study focussed on FWP diurnal dynamics in Fig. 8. It shows the average daily cycle of *in situ* measurements (LWP, XWP) and radiometer-based FWP. In Fig. 8 FWP_{min} was initially calibrated with XWP. This is why all FWP-curves are within the XWP-range (-0.4 to -0.1 [MPa]) and only partially within the LWP-range (-1.2 to -0.3 [MPa]). Nevertheless, a comparison of the time dynamics in relative changes along the day is appropriate. All FWP-curves indicated from 5 am in the morning (dawning time; gray downward arrow in Fig. 8) an increased water demand by more negative water potential values. This wass in phase with *in situ* LWP dynamics showing an increase at the same time. However, XWP measured at the

tree stems reacted with a delay of several hours and the strongest tension increase occurred after 10 am (negative slope of brown curve in Fig. 8). During this time, FWP was at a constant level around -0.3 [MPa].

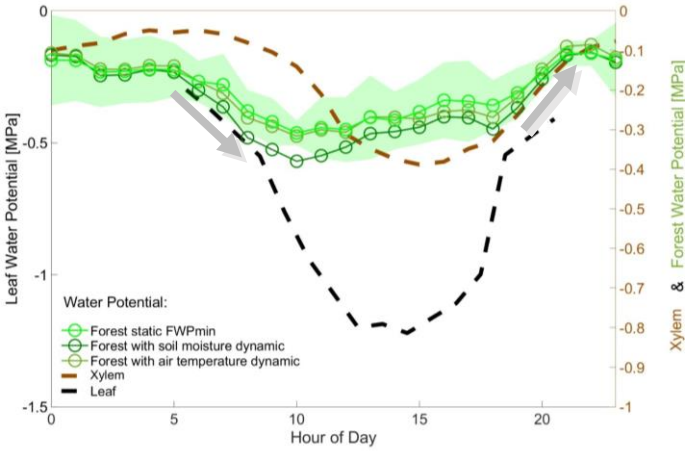

Fig. 8. Average daily cycle of water potentials: Estimated from remote sensing (FWP in green for static (bright) and dynamic FWP_{min} (middle and dark green)) and measured daily cycle of *in situ* water potentials: LWP (from leaves; black dashed line) and XWP (within the xylem; brown dashed line). Averaging was done over the intensive measuring period in July 2019. The green area shows the range over which the FWP from static FWP_{min} was averaged. Grey arrows indicate the starting and the ending phase of the diel dynamics of FWP.

After the heat maximum of the day (~ 2 pm) the water demand led to a decrease in LWP (leaves) first, followed by XWP (stems) at ~ 3 pm. The XWP curve showed a stronger decrease in water demand from ~ 6 pm onwards. At the same time FWP also started to move strongly towards reduced potential levels (gray upward arrow in Fig. 8). FWP dynamics (green curves in Fig. 8) coordinated in the morning with LWP (leaf dynamics) and in the evening with XWP (stem dynamics), implying that FWP is guided by leaf as well as by stem dynamics at the same time. This makes sense since FWP has a sensing volume including leaves, twigs and branches down to stems due to the sensing depth of L-band microwaves.

At daily timescale, results demonstrate how all three methods captured morning drying and post-dusk water rehydration in the forest stand (gray arrows in Fig. 8). Further work should be directed to extend the approach so that it can capture minimum midday XWP, which is a key hydraulic measurement in plant ecology research (e.g., Choat et al., 2012).

F. Weekly and monthly dynamics of FWP

Figure 9 shows the temporal extrapolation of FWP from July to September 2019 using the dynamic FWP_{min} updated by the measured soil moisture. Here, soil moisture was chosen, since transient changes of FWP_{min} over weeks from July to September 2019 are more attributed to soil moisture dynamics than to air temperature variations with a strong daily cycle at middle latitudes.

For reasons of unit equivalence, soil moisture was converted to soil matric potential [kPa]. These results are understood in the way that the trends and dynamics of FWP along the weeks match well with the measured XWP, except for large declines to very negative FWPs which are not captured by the proposed method in (7) (e.g., August 7th, or September 11th and 23rd).

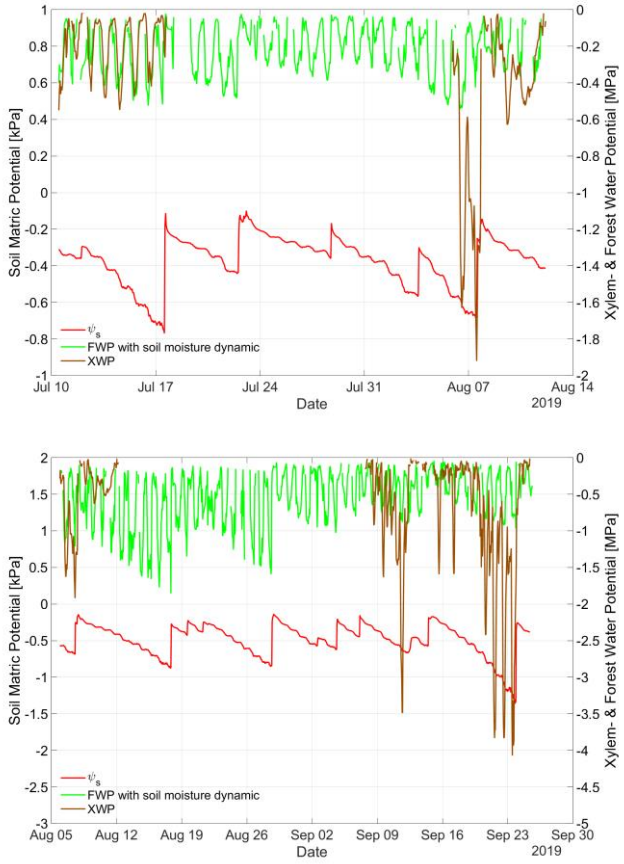

Fig. 9. Comparison of water potentials: FWP estimated from remote sensing with soil moisture-based FWP_{min} dynamics (in green color), XWP measured *in situ* (in brown color) and soil matric potential SMP estimated from soil moisture measurements (in red color).

This means that a potential extrapolation of the FWP time series and therefore conjunction of the different intensive measurement weeks by a soil moisture-updated FWP_{min} could extend the FWP estimations to months and seasons, but further investigations are needed to obtain an appropriate dynamic range of FWP.

V. Discussion

Understanding how plants transport and use water is key to monitor and predict the impact of droughts on vegetation and their exchange with the atmosphere (Zhang et al., 2019). According to Novick et al. (2022), there is a water potential information gap between ground-based observation networks and spatiotemporal scales relevant for Earth system models. This pathfinder study serves as a step towards addressing this gap and tracking water dynamics in the tree canopy over days, weeks and months. L-band radiometry was used for sensing the water dynamics of an oak stand at Harvard forest, USA, in the summer of 2019 as part of the SMAPVEX campaign.

The developed algorithm is based on a series of conversions to transform the radiometer-based, unitless *VOD* into absolute values of FWP. They include the conversion to relative water

content (VOD or m_g to RWC) and then from relative-to-absolute metric (RWC to FWP).

There are still challenges, but also considerable potential to derive and estimate microwave-based FWP. Previous research has shown the ability to track this site's xylem and leaf water potential (Holtzman et al., 2021). This study moved a step further, presenting conversion of VOD (microwave attenuation) to FWP (water potential) for a physically explicit assessment of water hydraulics in a forest stand from microwave radiometry. Results show how correlations between FWP estimates and XWP (*in situ*) are better (July) or only slightly lower (August and September) compared to the VOD-XWP correlation. This confirmed the potential utility of the method, providing such a conversion and tracking water potential in vegetation. In addition, the fact that FWP did not strongly improve the correlation with *in situ* water potential (if compared to VOD) was expected due to two shortcomings. First, VOD variations at short timescales are tightly linked to water status in the plants (Konings et al., 2021) and dry biomass dynamics were little during the study campaign, which qualifies VOD alone as a proxy to track the dynamics of water potentials (Feldman et al., 2021). In the case of agriculture, like in Jagdhuber et al. (2022), the growing cycle with its change in phenology (plant structure, height and biomass) from sowing to harvest required a decomposition of VOD into a plant water and a plant biomass component to effectively extract RWC. Such dynamics would result in a greater change in dry biomass and vegetation structure than occurring at Prospect Hill between July and September 2019.

Second, additional parameterization, needed to convert VOD to FWP, requires several data sources and adds additional uncertainty to the results (Zhao et al., 2024). A key step during the FWP estimation is the definition of the pressure-volume curves (cf. Fig. 4). The period used to compute maximum and minimum VOD or m_g for RWC calculation includes only three months, which hampers the possibility of accounting for extreme dry and wet periods. This is partially compensated for by the high density of samples, although longer time-periods should be studied to test the sensitivity of the method. Hence, one major drawback of this study is that *in situ* comparison data from xylem or leaf water potential were not recorded continuously along entire months, but for individual (unconnected) intensive measurement weeks. The resulting time gaps should be avoided, if possible in future campaigns.

Furthermore, although the pressure-volume curves are to some extent species-specific, the applied Zweifel et al. (2001) model was not directly optimized for oak species. The main reason for choosing the applied model relies on its adaptability and easy computation (dependence on a low number of parameters, cf. Section III). This qualifies the proposed RWC-to-FWP model as a candidate for future satellite-scale FWP estimates which will require generalizable, non-species-specific and low-parameterized methods.

Next steps for future satellite-based water potential estimates also involve the application of appropriate technologies to track plant water potential. In that sense, the future Copernicus Imaging Microwave Radiometer (CIMR) mission (Donlon, 2023; expected to launch in 2029+) will provide passive microwave measurements of the land surface at L-, C-, X-, K- and Ka-bands, offering different sensing depths and therefore different levels of canopy penetration, at an almost daily time scale globally. CIMR's consistent multi-frequency microwave measurements will potentially allow sensing water potential from different canopy layers (e.g., leaf water potential from xylem water potential), which is paramount for an appropriate understanding of the plant hydraulics and the soil-plant-atmosphere continuum. In addition, this can ease the validation process of water potential estimates, as *in situ* measurements are provided separately, for leaves or for xylem, and enable the study of plant hydraulics behavior at short (diel) time scales (Konings et al., 2021). For instance, the two in situ measurement networks VODnet (Schellenberg et al., 2024) and PSInet (https://psinetrcn.github.io/) for water potential as well as ground-based VOD retrieval through GNSS-T are under current construction increasing their number of equipped stations around the world. VODnet is already equipped with site-scale ground-based GNSS receivers for transmissometry assessment (Humphrey & Frankenberg, 2023). Ultimately, both networks are ideal testbeds to link tree measures to satellite data. In addition, similar approaches could be applied using GNSS reflectometry (GNSS-R) linking ground-based VOD and tree water content retrievals (Rodríguez-Álvarez et al., 2011) to satellite-based estimates of VWC from the Cyclone Global Navigation Satellite System (CYGNSS) mission (Zhang et al., 2024) and to *in situ* networks. However, it is worth noting that ground reflections in GNSS-R might complicate the estimation of canopy properties.

VI. Conclusions and Outlook

In this research study, a methodology is presented to estimate forest water potential (FWP) for an oak stand in the Harvard Forest based on ground-based L-band radiometry. A way was evaluated to generate time series of dynamic FWP starting from VOD and transitioning through m_g and RWC. The Zweifel et al. (2001) model was adapted to estimate time series of FWP. It is found that the incremental update of FWP_{min} in the adapted model (see (7) and (8)) is crucial to obtain a realistic range of values compared to the *in situ* observations of LWP and XWP and to estimate a continuous stream of FWP along weekly and monthly time scales.

FWP estimates showed the expected temporal dynamics, following the diurnal cycles and varying consistently with environmental drivers such as temperature. The correlation of the estimates with the *in situ* values confirmed the capacity of the method to track temporal variations in FWP. Consequently, this study provided a first valid approach to track vegetation water potential in a forest using the synergy between remotely sensed VOD and ancillary data through a model-based retrieval.

The achievement of absolute accuracy in FWP estimation still depends on the availability and quality of the auxiliary information. The needed accuracy will be defined in close coordination with the end users of FWP products. Here, mostly forest ecologists and tree physiologists will benefit from spatio-temporal water potential estimates from plot to ecosystem scales. In this regard, the presented approach builds the basic foundation for transitioning towards a remote sensing-based, up

to ecosystem-scale estimation of FWP dynamics with limited dependency on ancillary data. In the context of ecosystem-scale FWP retrievals, the current limitation of a mono-species (homogeneous oak stand) retrieval needs to be overcome. One of the next challenges is transferring the developed approach to the ecosystem scale, including various plant species representing different physiological traits.

Furthermore, FWP retrievals in this study cannot be separated into different vertical forest compartments, like trunks, branches, lower leaf (mostly shaded) canopy, upper leaf (mostly sunlit) canopy, due to the mono-frequency retrieval (only L-band). Upcoming microwave missions like NISAR (NASA-ISRO SAR) from the National Aeronautics and Space Administration (NASA) and the Indian Space Research Organization (ISRO), or BIOMASS and CIMR from the European Space Agency (ESA), will provide the possibility to acquire VOD globally and for different forest compartments (upper canopy, lower canopy, trunks) due to recordings of multi-frequency (K-, X-, C-, L- and P-band) microwave data at resolutions of tens of meters. However, research on VOD estimation from SAR (active microwave) techniques is still urgently needed to enable high resolution VOD and FWP products (e.g., El Hajj et al., 2019; Zhou et al., 2022).

ACKNOWLEDGMENT

D. Chaparro is funded by the projects 'la Caixa' Junior Leader Fellowship LCF/BQ/PI23/11970013 (lead: O. Binks) and H2020 FORGENIUS (Improving access to FORest GENetic resources Information and services for end-USers) #862221. D. Chaparro also received funding from the Ramón Areces Postdoctoral Fellowship. Andrew F. Feldman was supported by both the NASA ECOSTRESS science team and by a NASA Terrestrial Ecology scoping study for a dryland field campaign (ARID).

REFERENCES

Abrams, M. D., Adaptations and responses to drought in Quercus species of North America. *Tree Physiology*, 7, 227-238, 1990.

Anderegg, W. R. L., Wolf, A., Arango-Velez, A., Choat, B., Chmura, D. J., Jansen, S., Kolb, T., Li, S., Meinzer, F., Pita, P., Resco de Dios, V., Sperry, J. S., Wolfe, B. T., & Pacala, S. Plant water potential improves prediction of empirical stomatal models, *PLOS ONE*, 12, e0185481, 2017. https://doi.org/10.1371/journal.pone.0185481.

Balling, A. & Zimmermann, U. Comparative measurements of the xylem pressure ofNicotiana plants by means of the pressure bomb and pressure probe. *Planta*, 182, 325–338, 1990.

Barceló-Coll, J., Nicolás-Rodrigo, G., Sabater-García, B., & Sánchez-Tamés, R. Fisiología vegetal. 5th edition. Ediciones Pirámide S.A., Madrid, 1980.

Baur, M. J., Jagdhuber, T., Feldman, A. F., Akbar, R., & Entekhabi, D. Estimation of relative canopy absorption and scattering at L-, C-and X-bands. *Remote Sensing of Environment*, *233*, 111384, 2019.

Bonan, G. B., Williams, M., Fisher, R. A., & Oleson, K. W. Modeling stomatal conductance in the earth system: linking leaf water-use efficiency and water transport along the soil–plant–atmosphere continuum. *Geoscientific Model Development*, 7(5), 2193-2222, 2014.

Chaparro, D., Jagdhuber, T., Piles, M., Entekhabi, D., Jonard, F., Fluhrer, A., ... & Camps, A. Global L-Band Vegetation Volume Fraction Estimates for Modeling Vegetation Optical Depth. In *2021 IEEE International Geoscience and Remote Sensing Symposium IGARSS* (pp. 6399-6402). IEEE, 2021.

Chaparro, D., Jagdhuber, T., Piles, M., Jonard, F., Fluhrer, A., Vall-llossera, M., ... & Entekhabi, D. Vegetation moisture estimation in the Western United States using radiometer-radar-lidar synergy. *Remote Sensing of Environment*, *303*, 113993, 2024.

Choat, B., Jansen, S., Brodribb, T. J., Cochard, H., Delzon, S., Bhaskar, R., ... & Zanne, A. E. Global convergence in the vulnerability of forests to drought. *Nature*, 491(7426), 752-755, 2012.

Choat, B., Brodribb, T.J., Brodersen, C.R. et al. Triggers of tree mortality under drought. *Nature* 558, 531–539, 2018. https://doi.org/10.1038/s41586-018-0240-x.

Choudhury, B.J. & Pampaloni, P. eds., Passive Microwave Remote Sensing of Land--Atmosphere Interactions. CRC Press, VSP BV, The Netherlands, 1995.

Christoffersen, B. O., Gloor, M., Fauset, S., Fyllas, N. M., Galbraith, D. R., Baker, T. R., Kruijt, B., Rowland, L., Fisher, R.A., Binks, O. J., Sevanto, S., Xu, C., Jansen, S., Choat, B., Mencuccini, M., McDowell, N. G., & Meir, P.: Linking hydraulic traits to tropical forest function in a size-structured and traitdriven model (TFS v.1-Hydro), *Geosci. Model Dev.*, 9, 4227–4255, https://doi.org/10.5194/gmd-9-4227-2016, 2016.

Clark, M. A., Choi, J., & Douglas, M. *Biology 2e*. Rice University, 2018.

Colliander, A., et al., SMAP Detects Soil Moisture Under Temperate Forest Canopies, *Geophysical Research Letters*, 47(19), e2020GL089697, 2020.

Cowan I. Transport of water in the soil–plant–atmosphere system. *Journal of Applied Ecology*, 2: 221–239, 1965.

Chaparro, D., Jagdhuber, T., Piles, M., Jonard, F., Vall-llossera, M., Camps, A., López-Marínez, C., Fluhrer, A., Fernández-Morán, R., Baur, M., Feldman, A. F., Entekhabi, D. Estimation of gravimetric vegetation moisture in the western United States using a multi-sensor approach. In: 2023 *International Geoscience and Remote Sensing Symposium*. IEEE, 2023.

Dixon, M.A., & Tyree, M.T. A new stem hygrometer, corrected for temperature gradients and calibrated against the pressure bomb. *Plant, Cell & Environment*, 7, 693–697, 1984.

Donlon, C. J. The Copernicus Imaging Microwave Radiometer (CIMR) Mission Requirements Document v5. 0. Paris, France: ESA. https://cimr.eu/mrd_v5, 2023.

Edwards, D. R., & Dixon, M. A. Mechanisms of drought response in Thuja occidentalis LI Water stress conditioning and osmotic adjustment. *Tree Physiology*, 15(2), 121-127, 1995.

El Hajj, M., Baghdadi, N., Wigneron, J. P., Zribi, M., Albergel, C., Calvet, J. C., & Fayad, I. First vegetation optical depth mapping from

Sentinel-1 C-band SAR data over crop fields. *Remote Sensing*, *11*(23), 2769, 2019.

Eller, C. B., Rowland, L., Mencuccini, M., Rosas, T., Williams, K., Harper, A., Medlyn, B. E., Wagner, Y., Klein, T., Teodoro, G. S., Oliveira, R. S., Matos, I. S., Rosado, B. H. P., Fuchs, K., Wohlfahrt, G., Montagnani, L., Meir, P., Sitch, S., & Cox, P. M.: Stomatal optimization based on xylem hydraulics (SOX) improves land surface model simulation of vegetation responses to climate, *New Phytol*., 226, 1622–1637, 2020. https://doi.org/10.1111/nph.16419.

Entekhabi, D., et al., The soil moisture active passive (SMAP) mission, *Proceedings of the IEEE*, *98*(5), pp.704-716, 2010.

Entekhabi, D., et al., SMAP handbook–soil moisture active passive: Mapping soil moisture and freeze/thaw from space, 2014.

Feldman, A. F., Short Gianotti, D. J., Konings, A. G., Gentine, P., & Entekhabi, D. Patterns of plant rehydration and growth following pulses of soil moisture availability. *Biogeosciences*, 18, 831-847, 2021.

Forkel, M., Schmidt, L., Zotta, R. M., Dorigo, W., & Yebra, M. Estimating leaf moisture content at global scale from passive microwave satellite observations of vegetation optical depth. *Hydrology and Earth System Sciences Discussions*, 1-43, 2022.

Gardner, W. R. Dynamic aspects of water availability to plants, *Soil Sci*., 89, 63–73, 1960.

Gardner, W. R. Dynamic aspects of soil-water availability to plants, Ann. Rev. *Plant Physiol*., 16, 323–342, 1965.

Helman, D., Bahat, I., Netzer, Y., Ben-Gal, A., Alchanatis, V., Peeters, A., & Cohen, Y. Using time series of high-resolution planet satellite images to monitor grapevine stem water potential in commercial vineyards. *Remote Sensing*, *10*(10), 1615, 2018.

Holtzman, N., Konings, A.G., Roy, A., & Colliander, A., "*SMAPVEX19-21 Massachusetts Vegetation Optical Depth, Version 1*," [All]. Boulder, Colorado USA. NASA National Snow and Ice Data Center Distributed Active Archive Center. doi: https://doi.org/10.5067/2PZJDURUJLWF. [12.12.2020].

Holtzman, N. M., Anderegg, L. D., Kraatz, S., Mavrovic, A., Sonnentag, O., Pappas, C., ... & Konings, A. G. L-band vegetation optical depth as an indicator of plant water potential in a temperate deciduous forest stand. *Biogeosciences*, *18*(2), 739-753, 2021.

Humphrey, V., and Frankenberg, C. Continuous ground monitoring of vegetation optical depth and water content with GPS signals. *Biogeosciences*, 20, 1789-1811, 2023.

Hwang, T., Gholizadeh, H., Sims, D. A., Novick, K. A., Brzostek, E. R., Phillips, R. P., ... & Rahman, A. F. Capturing species-level drought responses in a temperate deciduous forest using ratios of photochemical reflectance indices between sunlit and shaded canopies. *Remote Sensing of Environment*, 199, 350-359, 2017.

Jackson, T. J., & Schmugge, T. J. Vegetation effects on the microwave emission of soils. *Remote Sensing of Environment*, *36*(3), 203-212, 1991.

Jagdhuber, T., Jonard, F., Fluhrer, A., Chaparro, D., Baur, M. J., Meyer, T., & Piles, M. Toward estimation of seasonal water dynamics of winter wheat from ground-based L-band radiometry: a concept study. *Biogeosciences*, *19*(8), 2273-2294, 2022.

Jonard F., André F., Ponette Q., Vincke C., & Jonard M. Sap flux density and stomatal conductance of European beech and common oak trees in pure and mixed stands during the summer drought of 2003. *Journal of Hydrology*, 409, pp. 371-381, 2011. http://dx.doi.org/ 10.1016/ j.jhydrol.2011.08.032.

Junttila, S., Hölttä, T., Puttonen, E., Katoh, M., Vastaranta, M., Kaartinen, H., ... & Hyyppä, H. Terrestrial laser scanning intensity captures diurnal variation in leaf water potential. *Remote Sensing of Environment*, *255*, 112274, 2021.

Kennedy, D., Swenson, S., Oleson, K. W., Lawrence, D. M., Fisher, R., Lola da Costa, A. C., & Gentine, P. Implementing Plant Hydraulics in the Community Land Model, Version 5, J. Adv. Model. Earth Sy., 11, 485–513, 2019. https://doi.org/10.1029/2018MS001500.

Kerr, Y. H., Waldteufel, P., Wigneron, J. P., Martinuzzi, J. A. M. J., Font, J., & Berger, M. Soil moisture retrieval from space: The Soil Moisture and Ocean Salinity (SMOS) mission. *IEEE transactions on Geoscience and remote sensing*, *39*(8), 1729-1735, 2001.

Konings, A. G., & Gentine, P. Global variations in ecosystem-scale isohydricity. *Global Change Biology*, 23(2), 891-905, 2017.

Konings, A. G., Rao, K., & Steele-Dunne, S. C. Macro to micro: microwave remote sensing of plant water content for physiology and ecology. *New Phytologist*, *223*(3), 1166-1172, 2019.

Konings, A. G., Saatchi, S. S., Frankenberg, C., Keller, M., Leshyk, V., Anderegg, W. R., ... & Zuidema, P. A. Detecting forest response to droughts with global observations of vegetation water content. *Global change biology*, *27*(23), 6005-6024, 2021.

Lambers, H., Stuart Chapin III, F., and Pons T. L.: Plant physiological ecology, Springer Science and Business Media, ISBN 9783030296391, 2008.

Li, X., Wigneron, J. P., Frappart, F., Fan, L., Ciais, P., Fensholt, R., ... & Moisy, C. Global-scale assessment and inter-comparison of recently developed/reprocessed microwave satellite vegetation optical depth products. *Remote Sensing of Environment*, 253, 112208, 2021.

Lin, Y., Zhu, Z., Guo, W., Sun, Y., Yang, X., & Kovalskyy, V. Continuous monitoring of cotton stem water potential using sentinel-2 imagery. *Remote Sensing*, 12(7), 1176, 2020.

Liu, Y., Kumar, M., Katul, G. G., Feng, X., and Konings, A. G. Plant hydraulics accentuates the effect of atmospheric moisture stress on transpiration, *Nat. Clim. Change*, 10, 691–695, 2020. https://doi.org/10.1038/s41558-020-0781-5.

Maherali H, Moura C.F., Caldeira M.C., Willson C.J., Jackson R.B. Functional coordination between leaf gas exchange and vulnerability to xylem cavitation in temperate forest trees. *Plant, Cell and Environment*, 29: 571-583, 2006.

Martínez-Vilalta, J. and Garcia-Forner, N.: Water potential regulation, stomatal behaviour and hydraulic transport under drought: deconstructing the iso/anisohydric concept, *Plant Cell Environ*., 40, 962–976, 2017.

Martínez-Vilalta, J., Anderegg, W. R., Sapes, G., & Sala, A. Greater focus on water pools may improve our ability to understand and

anticipate drought-induced mortality in plants, *New Phytol.*, 223, 22–32, 2019.

Matheny, A. M., Mirfenderesgi, G., & Bohrer, G. Trait-based representation of hydrological functional properties of plants in weather and ecosystem models. *Plant Div*., 39, 1–12, 2017.

McDowell, N., Pockman, W. T., Allen, C. D., Breshears, D. D., Cobb, N., Kolb, T., ... & Yepez, E. A. (2008). Mechanisms of plant survival and mortality during drought: why do some plants survive while others succumb to drought?. New phytologist, 178(4), 719-739.

Melcher, P.J., Meinzer, F.C., Yount, D.E., Goldstein, G. & Zimmermann, U. Comparative measurements of xylem pressure in transpiring and non-transpiring leaves by means of the pressure chamber and the xylem pressure probe. *Journal of Experimental Botany*, 49, 1757–1760, 1998.

Meyer T., Weihermüller L., Vereecken H., and Jonard F. Vegetation optical depth and soil moisture retrieved from L-band radiometry over the growth cycle of a winter wheat t. *Remote Sensing*, 10(10): 1637, 2018. http://dx.doi.org/10.3390/rs10101637.

Meyer, T., Jagdhuber T., Piles, M., Fink, A., Grant, J., Vereecken, H., & Jonard, F. Estimating gravimetric water content of a winter wheat field from L-band vegetation optical depth. *Remote Sensing*, *11*(20), 2353, 2019. https://doi.org/10.3390/rs11202353.

Mirfenderesgi, G., et al., Tree level hydrodynamic approach for resolving aboveground water storage and stomatal conductance and modeling the effects of tree hydraulic strategy, *Journal of Geophysical Research: Biogeosciences*, *121*(7), 1792-1813, 2016.

Mo, T., Choudhury, B. J., Schmugge, T. J., Wang, J. R., & Jackson, T. J. A model for microwave emission from vegetation-covered fields. *Journal of Geophysical Research: Oceans*, 87, 11229-11237, 1982.

Nolan, R. H., Blackman, C. J., de Dios, V. R., Choat, B., Medlyn, B. E., Li, X., Bradstock, R. A., & Boer, M. M.: Linking Forest Flammability and Plant Vulnerability to Drought, *Forests*, 11, 779, 2020. https://doi.org/10.3390/f11070779.

Novick, K. A., Ficklin, D. L., Stoy, P. C., Williams, C. A., Bohrer, G., Oishi, A. C., Papuga, S. A., Blanken, P. D., Noormets, A., Sulman, B. N., Scott, R. L., Wang, L., and Phillips, R. P.: The increasing importance of atmospheric demand for ecosystem water and carbon fluxes, *Nat. Clim. Change*, 6, 1023–1027, 2016. https://doi.org/10.1038/nclimate3114

Novick, K. A., Konings, A. G., & Gentine, P. Beyond soil water potential: An expanded view on isohydricity including land–atmosphere interactions and phenology. *Plant, cell & environment*, *42*(6), 1802-1815, 2019.

Novick, K. A., Ficklin, D. L., Baldocchi, D., Davis, K. J., Ghezzehei, T. A., Konings, A. G., ... & Wood, J. D. Confronting the water potential information gap. *Nature Geoscience*, *15*(3), 158-164, 2022.

Palmer AR, Fuentes S, Taylor D, Macinnis-Ng C, Zeppel M, Yunusa I, February E, Eamus D. Using pre-dawn leaf water potential and MODIS LAI to explore seasonal trends in the phenology of Australian and southern African woodlands and savannas. *Australian Journal of Botany*, 56: 557–563, 2008.

Palmer, A. R., Fuentes, S., Taylor, D., Macinnis-Ng, C., Zeppel, M., Yunusa, I., & Eamus, D. Towards a spatial understanding of water use of several land-cover classes: an examination of relationships amongst pre-dawn leaf water potential, vegetation water use, aridity and MODIS LAI. Ecohydrology: Ecosystems, Land and Water Process Interactions, *Ecohydrogeomorphology*, 3(1), 1-10, 2010.

Rao, K., Anderegg, W. R., Sala, A., Martínez-Vilalta, J., & Konings, A. G. Satellite-based vegetation optical depth as an indicator of drought-driven tree mortality. *Remote Sensing of Environment*, *227*, 125-136, 2019.

Rodriguez-Alvarez, N., Bosch-Lluis, X., Camps, A., Ramos-Perez, I., Valencia, E., Park, H., & Vall-Llossera, M. Vegetation water content estimation using GNSS measurements. *IEEE Geoscience and Remote Sensing Letters*, *9*, 282-286, 2011.

Rodriguez-Dominguez, C. M., Forner, A., Martorell, S., Choat, B., Lopez, R., Peters, J. M., ... & Sack, L. Leaf water potential measurements using the pressure chamber: Synthetic testing of assumptions towards best practices for precision and accuracy. *Plant, Cell & Environment*, 2022.

Rowlandson, T.L., et al., Capturing agricultural soil freeze/ thaw state through remote sensing and ground observations: A soil freeze/thaw validation campaign, *Remote Sensing of Environment*, *211*, 59-70, 2018.

Roy, A., et al., L-Band response to freeze/thaw in a boreal forest stand from ground-and tower-based radiometer observations, *Remote Sensing of Environment*, *237*, 111542, 2020.

Schellenberg, K., Jagdhuber, T., Chaparro, D., Binks, O., Hellwig, F., Dubois, C., Kurum, M., Camps, A., Hartmann, H., & Schmullius, C. Estimating Canopy Interception Water Storage with GNSS-Transmissometry. In *IEEE International Geoscience and Remote Sensing Symposium*, 4507-4510, 2024.

Schmidt, L., Forkel, M., Zotta, R. M., Scherrer, S., Dorigo, W. A., Kuhn-Régnier, A., ... & Yebra, M. Assessing the sensitivity of multi-frequency passive microwave vegetation optical depth to vegetation properties. *Biogeosciences*, 20(5), 1027-1046, 2023.

Schmugge, T. J., & Jackson, T. J. A dielectric model of the vegetation effects on the microwave emission from soils. *IEEE Transactions on Geoscience and Remote Sensing*, 30(4), 757-760, 1992.

Scholander, P. F., Bradstreet, E. D., Hemmingsen, E. A., & Hammel, H. T. Sap pressure in vascular plants: Negative hydrostatic pressure can be measured in plants. *Science*, 148(3668), 339–346, 1965. https://doi.org/10.1126/scien ce.148.3668.339

Slatyer, R. O. & Taylor, S. A.: Terminology in plant-and soil-water relations, *Nature*, 187, 922–924, 1960.

Smart, R.E., & Bingham, G.E., Rapid estimates of relative water content, *Plant physiology*, *53*(2), 258-260, 1974.

Sullivan, F.B., et al., Comparison of lidar-and allometry-derived canopy height models in an eastern deciduous forest, *Forest Ecology and Management*, *406*, 83-94, 2017.

Ulaby F.T., Razani M., & Dobson M.C. Effects of vegetation cover on the microwave radiometric sensitivity to soil moisture. *IEEE Transactions on Geoscience and Remote Sensing*, GE-21(1), 51-61, 1983.

Ulaby, F. T., & El-Rayes, M. A. Microwave dielectric spectrum of vegetation-Part II: Dual-dispersion model. *IEEE Transactions on Geoscience and Remote Sensing*, (5), 550-557, 1987.

Ulaby, F. & Long, D. *Microwave radar and radiometric remote sensing*, The University of Michigan Press, Michigan, USA, 2014.

Van den Honert, T.H. "Water transport in plants as a catenary process,". *Discussions of the Faraday Society*, *3*, 146-153,1948.

Venturas, M. D., Sperry, J. S., & Hacke, U. G. Plant xylem hydraulics: What we understand, current research, and future challenges: Plant xylem hydraulics, *J. Integr. Plant Biol.*, 59, 356–389, 2017. https://doi.org/10.1111/jipb.12534.

Wigneron J.P., Kerr Y., Chanzy A., Jin Y.Q. Inversion of surface parameters from passive microwave measurements over a soybean field. *Remote Sensing of Environment*, 46(1), 61-72, 1993.

Williams, A. P., Allen, C. D., Macalady, A. K., Griffin, D., Woodhouse, C. A., Meko, D. M., Swetnam, T. W., Rauscher, S. A., Seager, R., Grissino-Mayer, H. D., Dean, J. S., Cook, E. R., Gangodagamage, C., Cai, M., and McDowell, N. G. Temperature as a potent driver of regional forest drought stress and tree mortality, *Nat. Clim. Change*, 3, 292–297, 2013. https://doi.org/10.1038/nclimate1693.

Xu, X., Medvigy, D., Powers, J. S., Becknell, J. M., and Guan, K.: Diversity in plant hydraulic traits explains seasonal and inter-annual variations of vegetation dynamics in seasonally dry tropical forests, New Phytol., 212, 80–95, https://doi.org/10.1111/nph.14009, 2016.

Yebra, M., Scortechini, G., Badi, A., Beget, M. E., Boer, M. M., Bradstock, R., ... & Ustin, S. Globe-LFMC, a global plant water status database for vegetation ecophysiology and wildfire applications. *Scientific data*, 6(1), 155, 2019.

Yvon Duché, Y., Remi Savazzi, R., Toutchkov, M. and Cabanne, E. Multisite and multispecies live fuel moisture content (LFMC) series in the French Mediterranean since 1996 [Data set]. *Zenodo*, 2017. https://doi.org/10.5281/zenodo.162978

Zarco-Tejada P.J., Rueda, C.A., and Ustin, SL. 2003. Water content estimation in vegetation with MODIS reflectance data and model inversion methods. *Remote Sensing of Environment*, 85, 109–124, 2003.

Zarco-Tejada, P.J.; González-Dugo, V.; Williams, L.E.; Suárez, L.; Berni, J.A.J.; Goldhamer, D.; Fereres, E. A PRI-based water stress index combining structural and chlorophyll effects: Assessment using diurnal narrow-band airborne imagery and the CWSI thermal index. *Remote Sensing of Environment*, 138, 38–50, 2013.

Zhang, Y., Bu, J., Zuo, X., Yu, K., Wang, Q., & Huang, W. Vegetation Water Content Retrieval from Spaceborne GNSS-R and Multi-Source Remote Sensing Data Using Ensemble Machine Learning Methods. *Remote Sensing*, *16*, 2793, 2024.

Zhang, Y. J., Rockwell, F. E., Graham, A. C., Alexander, T., & Holbrook, N. M. Reversible leaf xylem collapse: a potential "circuit breaker" against cavitation. *Plant Physiology*, 172(4), 2261-2274, 2016.

Zhang, Y., Zhou, S., Gentine, P., & Xiao, X. Can vegetation optical depth reflect changes in leaf water potential during soil moisture dry-down events? *Remote Sensing of Environment*, *234*, 111451, 2019.

Zhao, M., Humphrey, V., Feldman, A. F., & Konings, A. G. Temperature is likely an important omission in interpreting vegetation optical depth. *Geophysical Research Letters*, e2024GL110094, *51*, 1-11, 2024.

Zhou, Z.; Fan, L.; De Lannoy, G.; Liu, X.; Peng, J.; Bai, X.; Frappart, F.; Baghdadi, N.; Xing, Z.; Li, X.; et al. Retrieval of High-Resolution Vegetation Optical Depth from Sentinel-1 Data over a Grassland Region in the Heihe River Basin. *Remote Sensing*, 2022, 14, 5468. https://doi.org/10.3390/rsl4215468

Zweifel, R., Item, H., & Häsler, R. Link between diurnal stem radius changes and tree water relations, *Tree physiology*, *21*(12-13), 869-877, 2001.